iEnergy
ARTICLE
https://doi.org/10.23919/IEN.2024.0008

An adaptive fuel cell hybrid vehicle propulsion sizing model

Jia Di Yang[1,2], Paul R. Shearing[3,4], Jason Millichamp[2], Theo Suter[1], Dan J. L. Brett[1,2,4] and James B. Robinson[1,2,4] ✉

ABSTRACT

As we enter the age of electrochemical propulsion, there is an increasing tendency to discuss the viability or otherwise of different electrochemical propulsion systems in zero-sum terms. These discussions are often grounded in a specific use case; however, given the need to electrify the wider transport sector it is evident that we must consider systems in a holistic fashion. When designed adequately, the hybridisation of power sources within automotive applications has been demonstrated to positively impact fuel cell efficiency, durability, and cost, while having potential benefits for the safety of vehicles. In this paper, the impact of the fuel cell to battery hybridisation degree is explored through the key design parameter of system mass. Different fuel cell electric hybrid vehicle (FCHEV) scenarios of various hydridisation degrees, including light-duty vehicles (LDVs), Class 8 heavy goods vehicles (HGVs), and buses are modelled to enable the appropriate sizing of the proton exchange membrane (PEMFC) stack and lithium-ion battery (LiB) pack and additional balance of plant. The operating conditions of the modelled PEMFC stack and battery pack are then varied under a range of relevant drive cycles to identify the relative performance of the systems. By extending the model further and incorporating a feedback loop, we are able to remove the need to include estimated vehicle masses *a priori* enabling improving the speed and accuracy of the model as an analysis tool for vehicle mass and performance estimation.

KEYWORDS

Proton exchange membrane (PEMFC), lithium-ion batteries, fuel cell electric hybrid vehicle (FCHEV), electric propulsion, powertrain modelling.

The widely legislated requirement for net-zero transport has increased the interest and development of electrochemical power sources including proton exchange membrane fuel cells (PEMFCs) and lithium-ion batteries (LiBs) for a range of automotive applications. When considered in isolation both power sources have a number of specific advantages and disadvantages, which, when considered in an appropriate manner allow the technologies to be applied in an application specific manner to maximise the utility and efficiency of a propulsion system. While it is undoubted that the majority of passenger electric vehicles will be powered by LiBs in the coming years. For these vehicles, LiB technology is well suited to deliver sufficient power over appropriate time scales, which when coupled with the higher efficiencies typically observed offer compelling performance and economic benefits. However, there are concerns around the sustainability of these systems which may provide a market opportunity for fuel cell electric vehicles (FCEVs) in this area over longer timeframes. Furthermore, the comparatively high gravimetric energy density and quick refuelling times of fuel cell (FC) systems may provide specific benefits for fleet and heavier vehicles and those primarily designed for extended range.

Table 1 shows a forecast of key design targets for automotive grade PEMFC systems up to 2035, with substantial improvements in the stack and system costs required, alongside enhanced system durability and efficiency[1]. While FCEVs are currently regarded by some as an overly expensive solution toward net-zero transportation[2], the improvements outlined by this development roadmap outline a path towards more competitive economics. These forecasted developments have a compounding impact when considered in a vehicle with improved system efficiency and durability reducing the cost and requirement for hydrogen generation and extending the potential cradle-to-grave impact of systems. Furthermore, the potential to recycle fuel cell components and systems has been demonstrated suggesting the longer term sustainability of this technology may be more readily achievable at scale than for LiB technologies[3].

Table 1 Roadmap for fuel cell vehicle light-duty vehicles (LDVs), adapted from APC fuel cell roadmaps[1]

	2020	2025	2035
System cost ($/kW)	112	68	40
Stack cost ($/kW)	70	40	20
System efficiency (%)	60	65	70
Stack durability (h)	5,000	6,000	8,000

While there are significant benefits expected in fuel cell technology, it is undoubted that battery technology will also continue to develop in the same timeframes. These expected improvements in cell and system performance are detailed in Table 2 which shows forecasts of battery technology at the cell and pack level.[4] Alongside this there is an expectation that the higher volumes of production which are expected will result in reduced cell and pack costs, and the significant focus on automotive applications will result in improvements in the charging times for systems. How-

[1]Electrochemical Innovation Lab, Department of Chemical Engineering, University College London, London WC1E 7JE, UK; [2]Advanced Propulsion Lab, Marshgate, University College London, London E20 2AE, UK; [3]ZERO Institute, Holywell House, Osney Mead, University of Oxford, Oxford, OX2 0ES; [4]The Faraday Institution, Quad One, Becquerel Avenue, Harwell Science and Innovation Campus, Didcot OX11 0RA, UK
Address correspondence to James B. Robinsona, j.b.robinson@ucl.ac.uk

Table 2 Roadmaps for battery electric vehicle (BEV) LiBs, adapted from APC electrical energy storage roadmaps[4]

	2020	2025	2030	2035
Cell level transient discharge power density ($W \cdot kg^{-1}$)	1100	1180	1260	1340
Gravimetric cell energy density ($Wh \cdot kg^{-1}$)	280	300	320	340
Volumetric cell energy density ($Wh \cdot L^{-1}$)	720	770	850	900
Cell cost ($\$ \cdot kWh^{-1}$)	85	70	58	48
Pack level transient discharge power density ($W \cdot kg^{-1}$)	715	825	945	1070
Pack C-rate	1.5	2.5	3.5	4
Gravimetric pack energy density ($Wh \cdot kg^{-1}$)	185	210	240	275
Volumetric pack energy density ($Wh \cdot L^{-1}$)	470	540	640	720
Pack cost ($\$ \cdot kWh^{-1}$)	125	97	77	63

ever, even if the projected improvements in battery and fuel cell technologies are realised, applications well suited to hybridisation will remain. This approach allows the benefits of both technologies to be leveraged, with the challenges associated with each individual solution mitigated at a full system level.

The challenge in moving towards a widespread electrification of vehicles involves converting existing systems including heavy goods vehicles, buses and beyond which require comparatively high specific energy and power density, adequate transient response times for power delivery and very long range[5]. In these applications, it is clear that there is a need to move beyond the capability of existing LiBs and as a result of this there is a substantial commercial interest in exploring the application of hybridised fuel cell/battery vehicles. These systems often do not have the volumetric constraint associated with electric vehicles which reduce the viability of hybridised systems in passenger EVs. By undertaking a considered hybridisation, it is possible to maximise the benefits of the battery and fuel cell systems on board, delivering long-range propulsion over appropriate lifetimes with acceptable power response. Further, in extending the lifetime of the propulsion system, when compared to a single technology in isolation, it is also possible to amortise the cost of the system over a longer duration reducing the overall operating costs of the vehicle for users[2,6].

In general, there are three main architectures of hybrid vehicles, namely series, parallel and series parallel[6,7]. In a series architecture, only one power source propels the wheels of a vehicle, while the other source is used for recharging the main propulsive power source; when using a parallel architecture, both power sources can propel the wheels[6,7]. The series-parallel architecture combines both architectures, in which both sources can provide traction while keeping the capability of one source charging another source. The motor can work in both directions, both as a propelling motor and a generator. Regenerative braking is possible in all architectures, during regen, the motor operates in reverse and acts as a generator, which provides recharge to the battery pack. The powertrain layout modelled in this study is the parallel layout, in which both the PEMFC stack and LiB pack can propel the vehicle independently with the PEMFC not recharging the battery.

A key aspect of developing a hybridised system is determining an appropriate hybrid degree (HD), a measure of the fuel cell system power output to the total required power of a vehicle. In the most widely popularised FC hybrid vehicle, the Toyota Mirai, the HD is around 0.71[8,9]; however, this will vary significantly when determining the requirements of a vehicle including the size of a system, range, lifetime and cost. Determining an appropriate operating power for the system is also a significant requirement in the hybridisation of the vehicle as operating at higher powers can reduce the mass (and extend the efficiency of the vehicle) at a cost to the lifetime.

A MATLAB model, HybeMass, is developed; this model examines both the hybridisation degree and cell operating power, identifying the requirements for PEMFC and LiB cell numbers, and overall power system and gross vehicle mass (GVM). Typically, automotive engineering follows the V-model concept, which begins with full vehicle conception and moves to module and component design and simulation, and finally component and full vehicle testing. In this work, the introduction of a feedback loop in the proposed the HybeMass MATLAB model to improve the efficiency of the V-model process for module and component design and simulation, specifically eliminating the need for a priori understanding of the vehicle's power demand. Identifying the optimal HD to minimise the vehicle's mass which can be used as a key design factor to extend the range. Figure 1 shows a generic automotive engineering V-model[10], a standardised method of vehicle development used by automotive manufacturers; the boxes with the dashed lines show the steps where the HybeMass mode may be capable of shortening or removing some of the steps in the vehicle design and testing process. The left side of the 'V' typically involves simulation and software use, while the right side of the 'V' typically involves physical implementation and testing. Engineers and the research and development (R&D) team typically need to step back to the left side of the 'V' during physical testing and implementation stages if something wasn't designed or engineered adequately; improper vehicle sizing may cause a step backward during these design stages. It is far more time and cost-efficient to ensure the sizing issues are addressed in the software and simulation changes (left V); the HybeMass software aims to remove sizing issues before reaching the physical testing and implementation stages. Although not highlighted in Figure 1, problems with sizing may still occur during the system verification stage. This stage is the second-last stage before a vehicle is subject to mass manufacturing, identifying sizing issues at this late stage may induce major developmental setbacks. It is crucial to address the sizing complication early.

Another example of a previous fuel cell hybrid electric vehicle (FCHEV) sizing design methodology is shown in Figure 2, proposed by Cai et al.[11] Similar to the previous figure regarding the automotive engineering V-model, the steps in which the HybeMass model could benefit are boxed in dashed lines. The last two steps are of interest, where the volume and mass of the energy storage system (battery pack) and fuel cell system are designed, and the suitability of them supporting the vehicle requirements needs to be validated. Again, it is beneficial to address and validate the sizing issue early to avoid any setbacks; the HybeMass model is capable

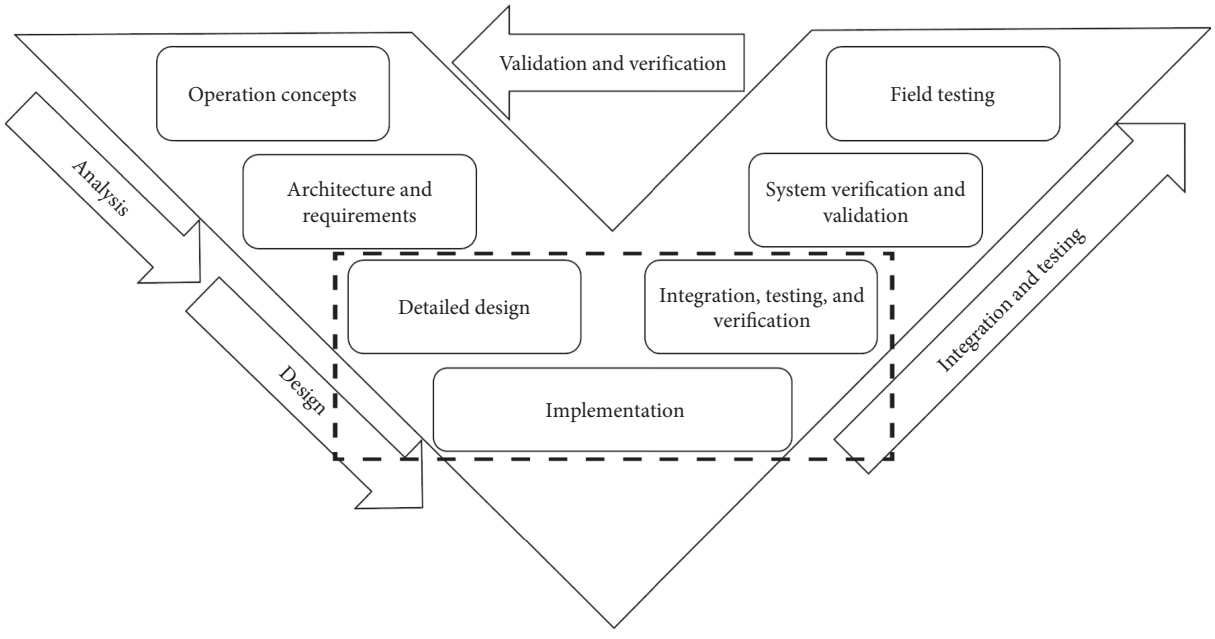

Figure 1 Generic automotive engineering V-model. The dashed box outlines the steps where the HybeMass model may increase the efficiency of the overall design process.

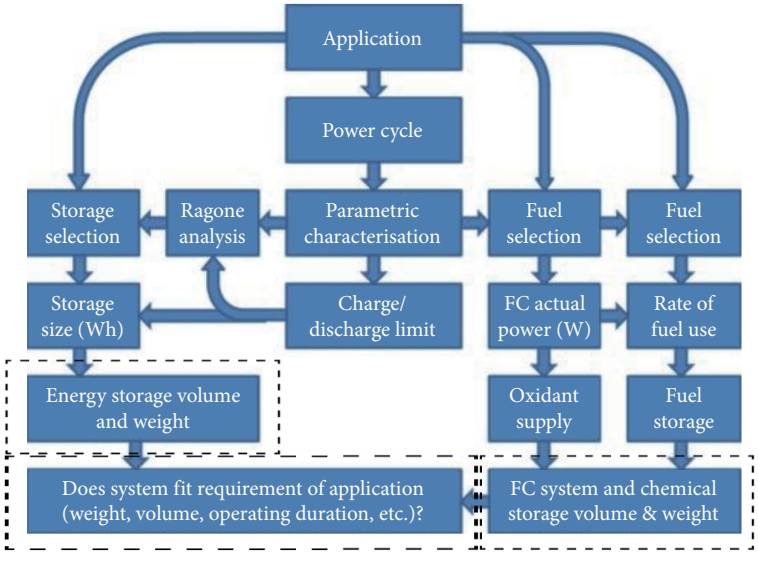

Figure 2 FCHEV sizing design methodology flow chart. Reprinted with permission from Ref. [11] © 2010 Elsevier.

of resolving this during earlier stages including the storage selection, storage size, charge and discharge limit, fuel cell selection, FC actual power, and fuel storage steps outlined in the figure.

Transient drive cycles are used to estimate the power demands of vehicles of different scenarios to determine the appropriateness of the suggested system for light-duty vehicles (LDV), Class 8 heavy goods vehicles (HGVs), and bus applications. To ensure accuracy parasitic component masses, auxiliary power draw, and efficiency losses are also considered in the relevant systems within the model.

This study focuses on the sizing and mass analysis of propulsions systems for FCHEVs of all vehicle classes rather than providing information regarding the required energy split or management strategies (EMS) of such vehicles which is heavily dependent upon use case and therefore unlikely to be generalised for the analysis type detailed here. There is an abundance of literature on optimising the EMS that a vehicle uses, but such studies tend not to elaborate on how the vehicle was sized before the application of EMSs. Usually, sizing is pre-determined without explanation or selected from a pre-built vehicle. Table 3 shows a review of selected publications that focus on the modelling of FCHEV or net-zero hybrid vehicles of different vehicle types (LDV, HGV, bus, tram) with emphasis on EMS and sizing studies. The table also outlines the power source sizing and hybrid architectures of the studies. Zhang et al.[12] utilised a FCHEV model in MATLAB to study the effects of three different EMSs for a range extender FCHEV LDV. The PEMFC stack and LiB pack specifications and cell count are pre-determined in the model based on a real FCHEV. The predetermined PEMFC stack and LiB pack are rated at powers and capacities of 8.3 kW and 77.33 Ah, respectively. Luca et al.[13] compared five different EMSs on a FCHEV LDV with a pre-determined PEMFC stack and LiB pack size of 25.5 kW and 11.1 kWh, respectively. The comparison was computed based on the powertrain simulation framework (EV-SimKit) created in MATLAB. Snoussi et al.[14]

Table 3 Literature review of past FCHEV and hybrid vehicle modelling literature with emphasis on EMS and power source sizing

Authors	Focus of study	Power source sizing	Hybrid architecture	Vehicle type
[12]	EMS	8.3 kW PEMFC; 77.33 Ah LiB	Range extender	LDV
[13]	EMS	25.2 kW PEMFC; 11.1 kWh LiB	Parallel	LDV
[14]	EMS	1.2 kW PEMFC; 40 Ah LiB; 3000F supercapacitor	Parallel	LDV
[15]	EMS	60 kW battery; 157 kW ICE	Parallel	LDV
[16]	EMS	300 kW PEMFC; 240 kW, 48 kWh (68 Ah) Ni-MH battery	Parallel	Tram
[17]	EMS	Two 127 kW PEMFC stacks; 450 kW Ni-MH battery	Parallel	Tram
[18]	EMS	50 kW PEMFC; 38 kW lead acid battery; 351.6 Wh SC	Parallel	LDV
[19]	EMS	210 PEMFC cells (power not specified); 5.9 Ah battery capacity; 55 F supercapacitor	Parallel	LDV
[20]	EMS	5 kW PEMFC; 11 kWh, 400 Ah LiB	Range extender	LDV
[8]	Sizing	40 kW PEMFC and 100 kW LiB; 40 kW PEMFC and 60 kW LiB; 60 kW PEMFC and 40 kW LiB; 80 kW PEMFC and 20 kW LiB; 100 kW PEMFC and 20 kW LiB	Parallel	LDV
[21]	Sizing	5 × 8 matrix of configurations	Series	Minibus
[22]	Sizing	Range of PEMFC sizing from 20 to 160 kW; 5.5 and 11 kWh LiB	Parallel	Bus
[23]	Sizing	80 kW PEMFC; 3.27 kWh Ni-MH battery	Parallel	LDV
[24]	Sizing	164 kW PEMFC; 54 kW,1.4 kWh LiB	Range extender and parallel	HGV
[25]	Sizing	20 different HDs	Series	SUV
[26]	Sizing	70 kW PEMFC; 50 kW, 100 Ah LiB	Parallel	Bus
[27]	Sizing	30 kW PEMFC; 12 kWh battery	Range extender	
[28]	EMS and sizing	35 kW PEMFC and 2.08 kWh SC; 29.1 kW PEMFC and 1.41 kWh SC; 31.9 kW PEMFC and 3.97 kWh SC; 26.9 kW PEMFC and 16.2 kWh SC	Parallel	Bus
[29]	EMS and sizing	Varying	Parallel	LDV

developed a powertrain model in MATLAB which studied the effects and optimisation of combining filtering-based EMS with fuzzy logic control (FLC) in a FCHEV LDV with a parallel PEMFC-LiB-supercapacitor drivetrain. A predetermined commercial PEMFC stack was chosen for the analysis, namely the Nexa Ballard 1.2 kW stack. A theoretical 40 Ah lithium iron phosphate (LFP) battery was pre-determined and modelled for the analysis.

By developing our HybeMass model we hope to enable the extension of these studies by enabling developers to explore the impact of the sizing of and HD of FCHEV's on the energy management. By providing this additional design consideration, our model will enable the optimisation of the system for the range and use case of vehicles, minimising the opportunities for overdesign in net-zero vehicles.

1 Methodology

A power source sizing and mass estimation model was developed from the ground-up in MATLAB Simulink, referred to hereafter as the HybeMass model. The model developed is composed of five subsystems: a power cycle convertor, parasitic losses and efficiency adjustments, cell count calculator, system mass feedback loop, and PEMFC diode and LiB overcharge protection. A flow diagram of the aforementioned subsystems is shown in Figure 3. The MATLAB program developed here 'self-updates' the newly added PEMFC and battery cell mass upon the pre-existing vehicle chassis mass to find the optimum number of cells needed to minimise the mass of the vehicle. The full formulation of the model is described in depth below.

The cell count calculator subsystem calculates the number of PEMFC and LiB cells required to support the vehicle, as well as

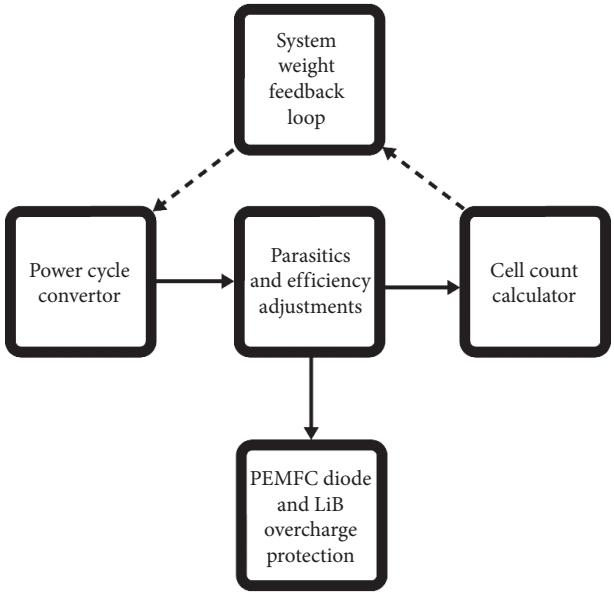

Figure 3 HybeMass model, general overview of subsystems.

calculating the PEMFC stack and LiB pack mass. In addition, the new gross vehicle mass (GVM) with power systems can be calculated. The power cycle convertor subsystem utilises vehicle design and powertrain development equations which will be outlined in further subsections (power cycle convertor subsystem) to convert a drive cycle to a power cycle. This converted power cycle only factors in tractive power and the mass of parasitic components, excluding the power draw by parasitic and auxiliary components. These losses and efficiency losses in the powertrain are obtained in

the next subsystem. Finally, the PEMFC diode and LiB overcharge protection subsystem, can be used to obtain separate power division profiles for the PEMFC stack and LiB pack. This subsystem extends beyond a simple arbitrary division of power with the model ensuring the PEMFC stack does not observe a negative voltage and the LiB pack is not overcharged within this system.

A simplified energy management system (EMS), percentage split, was used for the model. This approach assumes a linear division of required power between the PEMFC stack and LiB pack. For example, the PEMFC stack may account for 80% of the required power at a given second while the LiB pack accounts for the rest 20%, suggesting a 0.8 HD. As the proposed study focuses on the mass and HD of systems, the EMS is kept simple to allow consistency and accuracy. There are more dedicated EMSs for PEMFC-battery hybrid vehicles in literature, such as equivalent consumption minimisation strategy (ECMS), fuzzy logic control (FLC), and rate limited power (RLP) control[13]. Dedicated EMS may prolong PEMFC or LiB durability; however, they may skew the HD. This is a particular challenge for approaches including RLP, which rarely use the PEMFC stack at peak efficiency[13]. The percentage split approach deployed in this work ensures that the system is performing at the HD intended.

1.1 Power cycle convertor subsystem

To estimate power demands for the vehicle intended, drive cycles are transformed into power cycles. The drive cycles used include worldwide harmonised light vehicles test cycle (WLTC) Class 3, world harmonised vehicle cycle (WHVC), and orange county bus cycle (OC BUS), representing the velocity profiles of a LDV, HGV, and bus driving. This conversion is undertaken by calculating three individual force components shown in in Figure 4, namely aerodynamic drag (F_a), rolling resistance (F_r), and inertial force (F_i) which are then summed. This is then multiplied by velocity values to obtain a time resolved power demand. Due to the lack of angular data in standardized drive cycles the gradient force is omitted in this work. The aerodynamic drag force, which is a function of the velocity of the vehicle and a range of design criteria was calculated using:

$$F_a = \frac{1}{2}\rho c_d A v^2 \quad (1)$$

where ρ is the air density of 1.225 kg m^{-1} at sea level and 15 °C , c_d is the air drag coefficient, A is the vehicle's frontal area, and v is the speed at a given time step[7].

The rolling resistance force (F_r) was calculated using:

$$F_r = mgc_{rr}\cos(\theta) \quad (2)$$

where m is the mass of the vehicle, g is gravitational acceleration, c_{rr} is the rolling resistance coefficient, and θ is the road gradient,

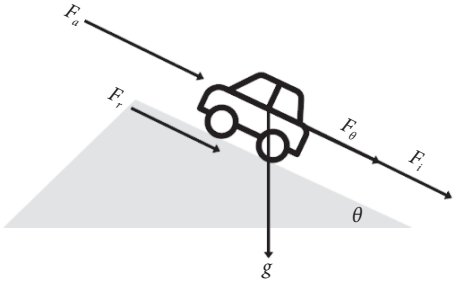

Figure 4 Converting a drive cycle to power cycle for power demand estimation.

which is omitted in drive cycle scenarios[7].

The inertial force (F_i) was calculated using:

$$F_i = ma \quad (3)$$

where a is the vehicle's acceleration.

Having calculated the constituent forces the overall force observed by the vehicle at a given velocity (F_{tot}) can be obtained as below[7]:

$$F_{tot} = F_a + F_r + F_i \quad (4)$$

This force can then be used to calculate the instantaneous power requirement (P_{req}) by multiplying the force by the speed shown in the drive cycle.

$$P_{req} = F_{tot} v \quad (5)$$

Due to the dynamic nature of the drive cycles, which include acceleration and deceleration the inertial force can provide a positive or negative value to the overall force, which, in turn provides an opportunity for the required power to be negative. In these instances, negative power enables regenerative braking to be introduced to further reduce the overall size of the system; however, it should be noted that this process introduces further inefficiencies. Here a factor of 0.8 was used to account for the losses associated with regenerative braking, this value is similar to that of a 2015 Nissan Leaf, as tested and has been further suggested by Fotouhi et al.[30].

Three types of vehicles were modelled using the HybeMass model: a LDV, Class 8 HGV (GVM > 15,000 kg), and bus. The parameters used for the LDV, HGV, and bus scenarios are presented in Table 4 with each vehicle scenario requiring specific inputs. Where possible, parameters from the fewest number of manufacturers possible have been chosen. Given the aim of the model to minimise the cell count, only the chassis and vehicle dynamic parameters were needed to be obtained from manufacturer specification sheets. The parameters were selected as close to the 2015 Nissan Leaf (chassis and vehicle dynamics parameters) and 2017 Toyota Mirai (hydrogen tank size and mass of hydrogen) for LDVs, and the Tesla Semi (chassis and vehicle dynamics parameters) for HGVs. The bus parameters were selected based on parameters estimated by Yang et al.[31], with the engine mass subtracted to provide an input for the chassis mass. The stored hydrogen mass for the HGV and bus is taken from previous commercially available vehicles of the same scenario, namely the Toyota Mirai and Hyundai Xcient Class 8 HGV or from previous literature analysing the same type of vehicle, for example, the bus's hydrogen mass (m_{H2}) of 11 kg[32]. Where commercial data was available, i.e. for LDVs, the hydrogen tank's mass (m_{tank}) was obtained from manufacturers' data sheets. The mass of hydrogen tanks for HGVs and buses is rarely published in data sheets as very few commercially available models exist. In this case, the gravimetric capacity (wt %) targets outlined by Department of Energy (DOE) was used to calculate the tank's mass from the hydrogen mass. The DOE estimates a target of 5.5 wt% for automotive-grade hydrogen storage for 2025[33]. Therefore, when calculated using the estimated hydrogen requirement of 35 kg and 11 kg for the HGV and bus, respectively, the mass of each tank was found to be 636 kg and 200 kg, respectively. Due to the early stage of deployment of FCHEVs, it is difficult to incorporate specifics regarding the hydrogen tank, especially in how much the weight of the tank would change between different hybrid degrees. For future work, a ratio between the different hybrid degrees could be implemented

Table 4 Vehicle mass and dynamic parameters for LDV, HGV, and bus scenarios[30–39,40]

Parameter	Vehicle type	Description	Value
C_d	LDV	Drag coefficient	0.28
A	LDV	Frontal area (m^2)	2.27
GVM	LDV	Gross vehicle mass (kg)	1780
m_{tank}	LDV	Mass of hydrogen tank (kg)	87.5
m_{H2}	LDV	Mass of hydrogen contained (kg)	5
m_{batt}	LDV	Mass of battery in commercial vehicle (kg)	151
C_d	HGV	Drag coefficient	0.36
A	HGV	Frontal area (m^2)	9
GVM	HGV	Gross vehicle mass (kg)	37195
m_{tank}	HGV	Mass of hydrogen tank (kg)	636
m_{H2}	HGV	Mass of hydrogen contained (kg)	35
m_{batt}	HGV	Mass of battery in commercial vehicle (kg)	2293
C_d	Bus	Drag coefficient	0.65
A	Bus	Frontal area (m^2)	7.78
GVM	Bus	Gross vehicle mass (kg)	17600
m_{tank}	Bus	Mass of hydrogen tank (kg)	200
m_{H2}	Bus	Mass of hydrogen contained (kg)	11
m_{engine}	Bus	Mass of engine in commercial vehicle (kg)	1093

for the tank weight estimation. When running the model, a MATLAB setup file is to be executed before running the Simulink model to initialise the aforementioned parameters.

Automotive-grade commercial PEMFCs and LiBs were chosen to propel the vehicle in the MATLAB model. A commercial PEMFC stack from a 2017 Toyota Mirai was used to characterise the fuel cell in the model. The primary design parameter used in the sizing model was the maximum power of a cell, which, while not provided by the manufacturer's datasheets can be estimated from the maximum power of the stack and number of cells which form the stack (128 kW and 370 cells respectively) suggesting the maximum cell power is 346 W or 1.46 W cm^{-2} (237 cm^{-2} active area)[34,35].

For the LiB proportion of the powertrain the LG M50 cylindrical 21700s were chosen, the same cells are used in a 2022 Tesla Model 3 long-range model[41] with the specifications of the cell outlined in Table 5. A maximum continuous discharge power of 20 W (1C discharge) was estimated by the authors from cycling and characterising the cell via a Maccor battery cycler, and a maximum charging power of 12 W was estimated based on the manufacturer's specification sheets[42].

Cell operating power is another degree of freedom that can drastically affect the mass of an FCHEV. The Toyota Mirai and LG M50 cells can either run at maximum power or a nominal power to fulfil the power requirements of the vehicle. Here, we defined a nominal operating power to be half of the maximum power of the cells, which results in 173 W and 10 W for the Toyota Mirai PEMFC and M50, respectively. The maximum power of both the fuel cell stack and battery pack are unlikely to be used due to the accelerated degradation associated with this decision, however in this scenario the pack mass will be minimised. When running at a nominal power, the stack and pack mass naturally increases, however there is a corresponding improvement in system durability. The selection of the operating condition is a decision driven by a range of factors including cost, mass, and lifetime, so to assess a range of considerations four conditions were explored: maximum PEMFC power, maximum battery power (NPML), maximum PEMFC power, nominal battery power (MPNL), nominal PEMFC power, maximum battery power (NPML), and nominal PEMFC power, nominal battery power (NPNL) as outlined in Table 6.

To accurately reflect the power estimation in each scenario it is important to consider parasitic losses and auxiliary power draw of vehicles, including the wider fuel cell balance-of-plant (BoP) and battery pack components, infotainment, and climate control systems. The PEMFC and LiB BoP and parasitic components are estimated using a gravimetric cell-to-pack ratio (GCTP) approach. The GCTP is a ratio commonly used by the battery and BEV

Table 5 LG INR21700 M50 parameters for characterisation and MATLAB modelling[42]

Parameter	Specification
Capacity (Ah)	5
Nominal voltage (V)	3.63
Maximum charge c-rate at 25 °C (C)	0.7
Maximum continuous charge power (W)	12
Maximum continuous discharge power at 25 °C and 1C (W)	20
Mass (kg)	0.068

Table 6 Operational terminology and maximum power output of PEMFC and LiB cells

Operation terminology	Pemfc maximum power (W)	LiB maximum power (W)
MPML	20	20
MPNL	20	10
NPML	10	20
NPNL	10	10

industry to account for the extra mass the parasitic components may add. The GCTP ratio factors in components such as battery management systems (BMS), thermal management systems (TMS), metal cases, cabling, and beams[43]. Different manufacturers have different estimates for GCTP, a GCTP of 0.64 is used for this analysis, which is the estimate for a 2017 Tesla Model 3[43]. While the GCTP is a well-defined and understood parameter in BEV's the equivalent, gravimetric cell to stack ratio (GCTS), for fuel cell systems have not widely been reported yet. Here, this was estimated from data available from a Toyota Mirai. It has been reported a single cell in the Mirai has a mass of 102 g[44] with the full fuel cell system weighing 52 kg[31]. From this we can estimate an approximate GCTS for the Toyota Mirai system of 0.65. This does not include the mass of the hydrogen tank for fuel supply as this is incorporated at later stages of the model.

Figure 5 shows the schematics of the power cycle convertor subsystem of the HybeMass model. F_a, F_r, and F_i are calculated separately using Equations (1) to (3). The forces are each multiplied by the instantaneous velocity to determine the power required. The power values are then totalled to obtain the required power curve. The subsystem's computed results were then provided to the parasitics and efficiency adjustments subsystem, discussed in more detail in Section 1.3.

1.2 System mass feedback loop

The system mass feedback loop which has been developed for this model enables the optimal hybridised configuration for the vehicle, minimising the mass of the final system. Firstly, the required power can be defined as purely tractive power. The analysis can be further in depth as per simulation and design requirements. The tractive power required should equal to the total power the PEMFC stack and LiB pack can produce. A stack and pack is defined as the product of the power of a single PEMFC or LiB multiplied by the total number of PEMFC and LiB cells in the system, this equation is shown in Equation (6) below.

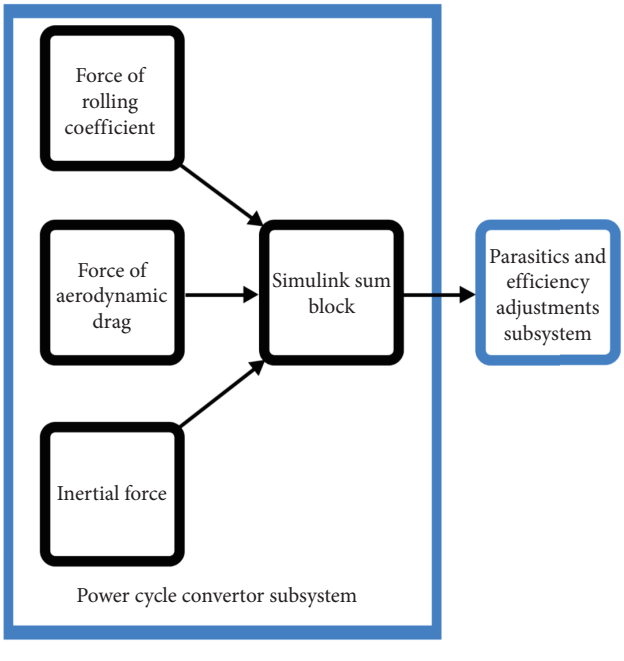

Figure 5 Model overview of power cycle convertor subsystem. This subsystem converts a drive cycle to a power cycle to determine the maximum required power of the proposed vehicle.

$$P_{\mathrm{PEMFC}} \times N_{\mathrm{PEMFC}} + P_{\mathrm{LiB_{cell}}} \times N_{\mathrm{LiB_{cell}}} = P_{\mathrm{req}} \tag{6}$$

where P_{PEMFC} and $P_{\mathrm{LiB_{cell}}}$ are the power output of a single PEMFC or LiB cell, respectively, this power can be rated at nominal or maximum (or in between), as discussed in Section 1.1. N_{PEMFC} and $N_{\mathrm{LiB_{cell}}}$ is the number of PEMFCs and LiB cells, respectively. P_{req} is the required power.

If only accounting for tractive power (P_{tractive}), the tractive power can be calculated using the power estimation method described in Section 1.1. The overall equation is shown in Equation (7).

$$\begin{aligned} P_{\mathrm{tractive}} &= F_{\mathrm{tot}} \times v = (F_a + F_r + F_i) \times v \\ &= \left(\frac{1}{2} \rho c_d A v^2 + m g c_{rr} \cos(\theta) + m a \right) \times v \end{aligned} \tag{7}$$

The singular PEMFC and LiB cells can operate at a nominal or maximum power, as explained in Section 1.1. The mass of the vehicle can be broken down into the mass of the vehicle's body (no power source components), $m_{v_{\mathrm{body}}}$, and the mass of the power sources, in this case, PEMFC stack and LiB pack, the mass of the stack and pack can be calculated as the number of cells (N_{PEMFC}, $N_{\mathrm{LiB_{cell}}}$) multiplied by a singular cell mass (m_{PEMFC}, $m_{\mathrm{LiB_{cell}}}$). N_{PEMFC} and $N_{\mathrm{LiB_{cell}}}$ are the parameters to be solved by these equations. The full equation is shown in Equation (8), which acts as the basis of the system mass feedback loop equation.

$$\begin{aligned} &P_{\mathrm{PEMFC}} \times N_{\mathrm{PEMFC}} + P_{\mathrm{LiB_{cell}}} \times N_{\mathrm{LiB_{cell}}} = \\ &\frac{1}{2} \rho c_d A v_{P_{\max}} + \left(m_{v_{\mathrm{body}}} + N_{\mathrm{PEMFC}} m_{\mathrm{PEMFC}} + N_{\mathrm{LiB_{cell}}} m_{\mathrm{LiB_{cell}}} \right) g c_{rr} v_{P_{\max}} + \\ &\left(m_{v_{\mathrm{body}}} + N_{\mathrm{PEMFC}} m_{\mathrm{PEMFC}} + N_{\mathrm{LiB_{cell}}} m_{\mathrm{LiB_{cell}}} \right) a_{P_{\max}} v_{P_{\max}} \end{aligned} \tag{8}$$

Where $a_{P_{\max}}$ and $v_{P_{\max}}$ is the acceleration and speed at the maximum required power time step, respectively.

1.3 Parasitics and efficiency adjustments

The aforementioned equations in Section 1.2 only account for tractive power of the vehicle and does not consider additional, parasitic mass introduced by the PEMFC and LiB systems. As discussed previously, additional components including cables, control and thermal management systems and housing/endplates are needed for the PEMFC stack and LiB pack to function properly. As mentioned in Section 2.1, GCTP and GCTS values are used to estimate the additional mass of the parasitic components. For a more detailed analysis, the system mass feedback equations should

account for the extra power required from the parasitic mass ($P_{m\text{parasitics}}$), shown in Equation (9).

$$P_{\text{PEMFC}} \times N_{\text{PEMFC}} + P_{\text{LiB}_{\text{cell}}} \times N_{\text{LiB}_{\text{cell}}} = P_{\text{tractive}} + P_{\text{mparasitics}} \quad (9)$$

By adding GCTP ratios to Equation (8), a new source power equating to required power equation is shown in Equation (10). In this equation, P_{req} is now added with the parasitics mass, accounted for by GCTP and GCTS ratios. The GCTS and GCTP ratios are accounted for separately in m_{PEMFC} and $m_{\text{LiB}_{\text{cell}}}$ fields. For simplicity, the terms '$\frac{N_{\text{PEMFC}} m_{\text{PEMFC}}}{GCTS_{\text{PEMFC}}}$, and '$\frac{N_{\text{LiB}_{\text{cell}}} m_{\text{LiB}_{\text{cell}}}}{GCTP_{\text{LiB}}}$, will be called m_{stack} and m_{pack} in further mentioned equations, respectively.

$$\begin{aligned} &P_{\text{PEMFC}} \times N_{\text{PEMFC}} + P_{\text{LiB}_{\text{cell}}} \times N_{\text{LiB}_{\text{cell}}} = \\ &\frac{1}{2}\rho c_{\text{d}} A v_{P_{\max}} + \left(m_{v_{\text{body}}} + \frac{N_{\text{PEMFC}} m_{\text{PEMFC}}}{GCTS_{\text{PEMFC}}} + \frac{N_{\text{LiB}_{\text{cell}}} m_{\text{LiB}_{\text{cell}}}}{GCTP_{\text{LiB}}} \right) g c_{\text{rr}} v_{P_{\max}} + \\ &\left(m_{v_{\text{body}}} + \frac{N_{\text{PEMFC}} m_{\text{PEMFC}}}{GCTS_{\text{PEMFC}}} + \frac{N_{\text{LiB}_{\text{cell}}} m_{\text{LiB}_{\text{cell}}}}{GCTP_{\text{LiB}}} \right) a_{P_{\max}} v_{P_{\max}} \end{aligned} \quad (10)$$

The PEMFC stack or LiB pack's total power should equal to the required power allocated by the HD. The HD suggests to the ratio split of the PEMFC stack or battery pack. Since HD is defined as the power of the PEMFC to the total power, the ratio split of the LiB pack can be defined as $1 - \text{HD}$. The two separate equations for the PEMFC and LiB are shown in Equations (11) and (12).

$$\begin{aligned} &P_{\text{PEMFC}} \times N_{\text{PEMFC}} = \\ &\left[\frac{1}{2}\rho c_{\text{d}} A v_{P_{\max}} + \left(m_{v_{\text{body}}} + m_{\text{stack}} + m_{\text{pack}} \right) g c_{\text{rr}} v_{P_{\max}} + \right. \\ &\left. \left(m_{v_{\text{body}}} + m_{\text{stack}} + m_{\text{pack}} \right) a_{P_{\max}} v_{P_{\max}} \right] \times HD \end{aligned} \quad (11)$$

$$\begin{aligned} &P_{\text{LiB}_{\text{cell}}} \times N_{\text{LiB}_{\text{cell}}} = \\ &\left[\frac{1}{2}\rho c_{\text{d}} A v_{P_{\max}} + \left(m_{v_{\text{body}}} + m_{\text{stack}} + m_{\text{pack}} \right) g c_{\text{rr}} v_{P_{\max}} + \right. \\ &\left. \left(m_{v_{\text{body}}} + m_{\text{stack}} + m_{\text{pack}} \right) a_{P_{\max}} v_{P_{\max}} \right] \times (1 - HD) \end{aligned} \quad (12)$$

The realistic application of the equation can be improved further by factoring accessory load values (P_{acc}) and efficiency losses such as DC/DC convertor loss. The new equation for P_{req} is shown in Equation (13).

$$P_{\text{PEMFC}} \times N_{\text{PEMFC}} + P_{\text{LiB}_{\text{cell}}} \times N_{\text{LiB}_{\text{cell}}} = P_{\text{tractive}} + P_{m_{\text{parasitics}}} + P_{\text{acc}} \quad (13)$$

Equation (14) shows the equation used to factor in parasitics and accessory load and efficiency losses[44].

$$P_{\text{req}} = P_{\text{tractive}} / \eta_{\text{inv}} + P_{\text{acc}} / \eta_{\text{dc}} \quad (14)$$

Where η_{inv} and η_{dc} are the efficiency factors for the invertor and DC/DC convertor, respectively. P_{acc} is the parasitics and accessory load power draw. In the case of the LDV, the maximum parasitic and accessory load power draw is 12.9 kW, with the breakdown of these loads shown in Table 7. This analysis considers the worst-case scenario of the power draw. In reality, an FCHEV LDV uses a fraction of this at any given time with an estimated average of 5 kW used in LDV applications for the parasitic and accessory loads[45]. This data is not widely available for bus and HGV scenarios, therefore in this model the estimated power loading has been scaled to 12.5 and 20 kW, respectively, based on the mass of the vehicles. These efficiency and accessory load values make up the bulk of the parasitic and efficiency loss subsystem. The subsystem also contains a regenerative braking factor of 0.8 to adjust for charging losses[30].

Table 7 Breakdown and estimate of parasitic and auxiliary power draw for an FCHEV LDV, values adapted from Lawrence et al.[46]

Component	Power (W)
Exterior lights	175
Headlights	125
Interior lights	64
Windshield wipers	64
Power windows	180
AC compressor	4000
Cabin heater	3000
Cooling fans	400
Cabin blower	250
Cooling pumps	180
Rear defog	150
12 V battery charging	120
PEMFC cooling pump	600
PEMFC recirculating pumps	400
Motor lube pumps	120
PEMFC blower	2000
Power steering	800
Vacuum pumps	200
Controllers, relays, and contractors	100

The total required power is now updated with parasitics and accessory power draw and efficiency factors, shown in Equation (15).

$$P_{\text{PEMFC}} \times N_{\text{PEMFC}} + P_{\text{LiB}_{\text{cell}}} \times N_{\text{LiB}_{\text{cell}}} = \left(\frac{P_{\text{tractive}} + P_{m_{\text{parasitics}}}}{\eta_{\text{inv}}} + P_{\text{acc}} \right) / \eta_{\text{dc}} \quad (15)$$

The final equations to obtain N_{PEMFC} and $N_{\text{LiB}_{\text{cell}}}$ was updated with tractive power, power caused by additional mass of the parasitics (BoP and battery system components), power of parastics and auxiliary power draw, and efficiency loss factors. Equations (16), (17), and (18) show the updated and final versions of the goal seek equation. Equation (16) represents the overall power system power output, while Equations (17) and (18) represent the PEMFC stack and LiB pack power output, respectively.

$$\begin{aligned} &P_{\text{PEMFC}} \times N_{\text{PEMFC}} + P_{\text{LiB}_{\text{cell}}} \times N_{\text{LiB}_{\text{cell}}} = \\ &\left\{ \left[\frac{1}{2}\rho c_{\text{d}} A v_{P_{\max}} + \left(m_{v_{\text{body}}} + m_{\text{stack}} + m_{\text{pack}} \right) g c_{\text{rr}} v_{P_{\max}} + \right. \right. \\ &\left. \left. \left(m_{v_{\text{body}}} + m_{\text{stack}} + m_{\text{pack}} \right) a_{P_{\max}} v_{P_{\max}} \right] / \eta_{\text{inv}} + P_{\text{acc}} \right\} / \eta_{\text{dc}} \end{aligned} \quad (16)$$

$$\begin{aligned} &P_{\text{PEMFC}} \times N_{\text{PEMFC}} = \\ &\left\{ \left[\frac{1}{2}\rho c_{\text{d}} A v_{P_{\max}} + \left(m_{v_{\text{body}}} + m_{\text{stack}} + m_{\text{pack}} \right) g c_{\text{rr}} v_{P_{\max}} + \right. \right. \\ &\left. \left. \left(m_{v_{\text{body}}} + m_{\text{stack}} + m_{\text{pack}} \right) a_{P_{\max}} v_{P_{\max}} \right] / \eta_{\text{inv}} + P_{\text{acc}} \right\} / \eta_{\text{dc}} \times HD \end{aligned} \quad (17)$$

$$P_{\text{LiB\_cell}} \times N_{\text{LiB\_cell}} = \left\{ \left[\frac{1}{2}\rho c_{\text{d}} A v_{P_{\max}} + \left(m_{v_{\text{body}}} + m_{\text{stack}} + m_{\text{pack}}\right) g c_{\text{rr}} v_{P_{\max}} + \left(m_{v_{\text{body}}} + m_{\text{stack}} + m_{\text{pack}}\right) a_{P_{\max}} v_{P_{\max}} \right] / \eta_{\text{inv}} + P_{\text{acc}} \right\} / \eta_{\text{dc}} \times (1 - HD) \quad (18)$$

1.4 Cell count calculator and its synergy with other subsystems

The cell count subsystem is the constant update and display of the cell count calculated. Figure 6 shows the detailed connections and layout of the system mass feedback loop and cell count calculator subsystem, as well as its synergy with the power cycle convertor subsystem and parasitics and efficiency adjustments subsystem.

Two MATLAB function blocks are used to input equations 17 and 18. The solver functions are connected to these two equations to obtain a result for N_{PEMFC} and $N_{\text{LiB}_{\text{cell}}}$. The N_{PEMFC} and $N_{\text{LiB}_{\text{cell}}}$ values are constantly re-uploaded into the system mass feedback loop for recalculation of the power requirements and newly updated cell count. Every time N_{PEMFC} and $N_{\text{LiB}_{\text{cell}}}$ values update, the power requirements is directly affected due to the change in power systems mass, allowing a new power cycle to be obtained in the power cycle convertor subsystem. The parasitics and efficiency subsystem applies factors to the new power cycle, and the max power considering GCTS and GCTP factors, parasitics power draw, and efficiency losses are used to size the re-occurring PEMFC and LiB cell count (N_{PEMFC} and $N_{\text{LiB}_{\text{cell}}}$), This constant is updated constantly with the new maximum required power from

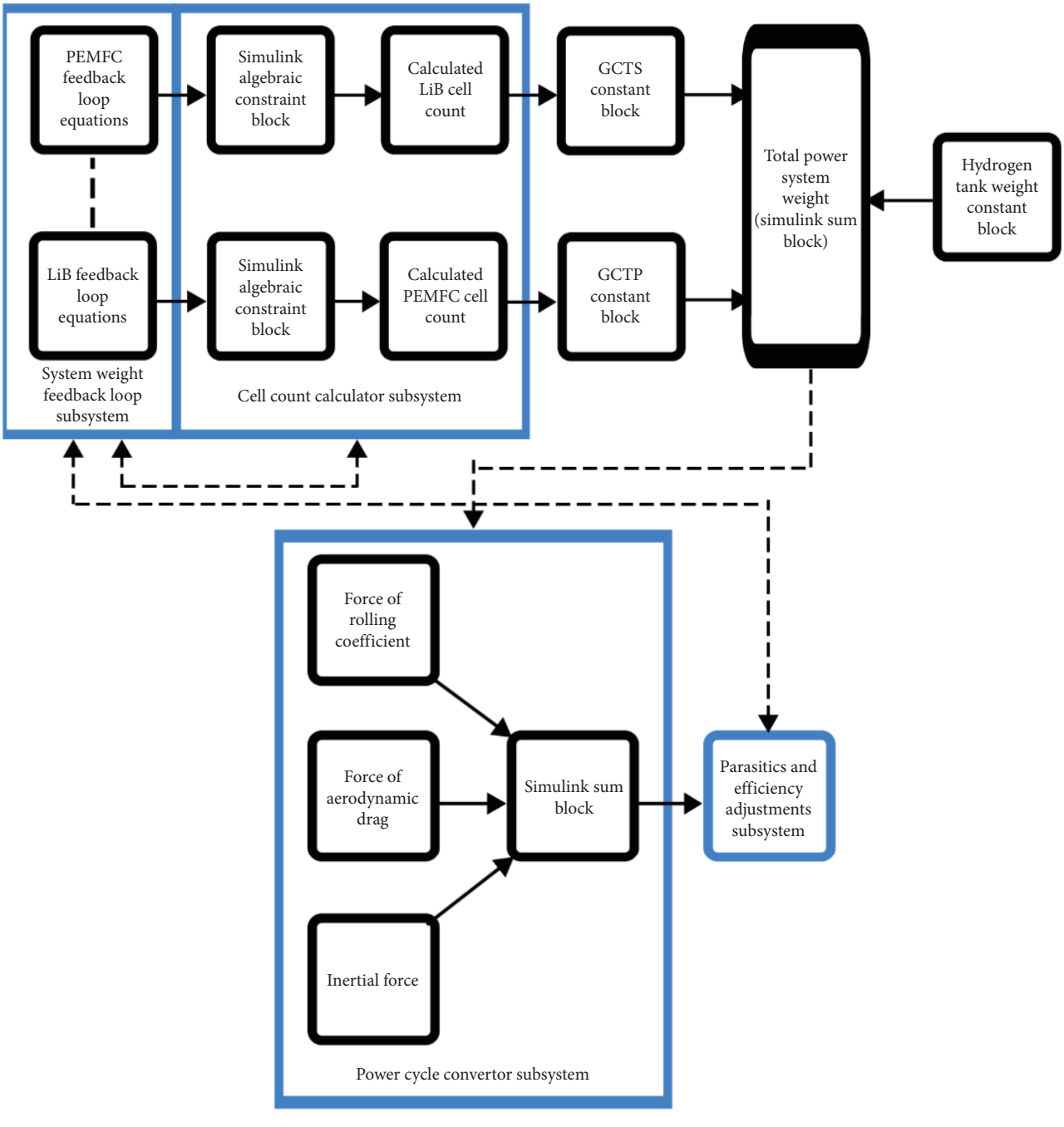

Figure 6 Detailed block layout of system mass feedback loop subsystem.

a 'To Workspace' block found in the power cycle convertor subsystem. Forming a loop of newly calculated required power accounting for the additional mass of the newly added PEMFC and LiB cells, realising the system mass feedback loop feature. After N_{PEMFC} and $N_{LiB_{cell}}$ are obtained, the mass of the PEMFC stack and battery stack can be obtained by multiplying the result by the destined singular cell mass; a GCTS or GCTP factor is then applied to account for parasitics mass. For the PEMFC stack counterpart, a pre-determined hydrogen tank mass can be added to the overall BoP and the overall power systems mass.

1.5 PEMFC diode and LiB overcharge protection subsystem

The diodes and overcharge protection subsystem is useful for exporting separate power cycles for the PEMFC stack and LiB pack. The exported power cycles can be used for further analysis such as bench or hardware-in-the-loop drive cycle testing. However, even with the pre-determined percentage split or EMS, there are some modifications that has to be applied to the power cycle to prevent charging the PEMFC stack or overcharging the LiB pack. The PEMFC stack power profile should never have a required power less than 0, while the LiB pack should not have a regen more than N_{LiB_cell} multiplied by the maximum charge power a M50 cell can take. Switches are implemented within the model to act as diodes and overcharge protection to prevent these safety issues. This subsystem is useful for exporting power profiles for the PEMFC stack and LiB pack so that these devices can be used for physical testing such as facilitating hardware-in-the-loop bench testing based on drive cycles.

2 Results and discussion

The results obtained from the model are presented below for three different vehicle scenarios, a LDV, Class 8 HGV, and bus. The overall mass of the propulsion system is broken down into five different power system components, LiB component mass (shown in yellow), LiB mass (green), hydrogen tank mass (blue), PEMFC component mass (orange), and PEMFC mass (black). By exploring different HDs for these vehicles it can be seen that the overall mass of the propulsion system reduces significantly as the extent of power delivered by the fuel cell increases. It is also clear that once a decision to hybridise a system is made the net mass change of the fuel cell system is relatively small when compared to the change in battery mass for all scenarios. It is clear from the results that operating a system with maximum PEM and LiB power (MPML) will provide the lowest system mass while the NPNL setup would most likely have the best durability. It is also evident that in some instances, a relatively low HD can increase the mass of the system, removing the most significant benefit assessed using this model. However, in general a trend is observed that reduces the overall system mass when hybridisation is considered. While the result suggest a HD of 1 is the lightest system, this solution has no LiBs included which is unlikely to be a satisfactory solution due to the accelerated degradation likely imposed on the PEMFC stack. In addition further BoP would be required to start the PEMFC's BoP. The PEMFC stack would be running at ambient conditions without a battery pack to power up BoP components such as heating cartridges, removing the ability to adjust for PEMFC operating parameters such as cell temperature and humidification. This may affect the performance of the stack.

2.1 LDV

Figure 7 presents the mass distributions for a LDV FCHEV, FCEV, and BEV under different HDs and cell operating powers. It can be seen with a 0.2 HD for MPML and NPML, hybridisation increases the mass of the power system by 8% and 10%, respectively, when compared to a full BEV setup. The added system complexity of hybridisation combined with the extra mass makes these setups unfeasible. Aside from these HDs at these cell operating points, the trend is that higher HDs result in lower power systems mass for LDVs.

Table 8 shows the change in mass of the power systems with increasing HDs for the four scenarios examined. These results highlight potential mass reductions range from 43% to 71% for the 0.8 HD when compared to the full BEV. The 0.8 HD is a common degree for commercially available FCEVs, similar to that of a Toyota Mirai (0.71 HD)[8,9].

The NPML cell operating power is the best setup to prolong the durability of both the PEMFC and LiB, while maintaining a feasible power system mass. LiBs tend to have higher dynamic response when compared to PEMFCs[45]. Having the PEMFC running at nominal powers would slow down its degradation rate and maximum power drop, as well as decreasing the transientness of the PEMFC power profile. Less transientness may prolong the lifetime of the PEMFC. A high level of transient operation accelerates the voltage decay of the PEMFC[46]. Gas lag and starvation are the main contributors causing the degradation of PEMFCs during dynamic loads, causing electrochemical surface area (ECSA) decrease[46]. LiB cells can cope with transient response better and experience less degradation when subjected to dynamic loads, allowing them to run at maximum operating power can bring mass saving benefits. In a commercial scenario, the LiB cells may need to be oversized or to be operated at a near maximum operating power instead of the absolute maximum to account for higher vehicle life expectancy. Even by running the PEMFCs at a nominal power at the popularised 0.8 HD, a 43% drop in mass is still expected when compared to a full BEV.

From Table 8, it can be seen the maximum propulsion system mass savings for the devices explored in this work when hybridising a LDV is 71% (0.8 HD MPNL). However, this scenario assumes a situation in which the fuel cell is operated at its maximum power with the LIB operating under nominal conditions. Operating a fuel cell at its maximum power will undoubtedly impact the durability, and by extension the lifetime cost of the propulsion system for the vehicle. It can be seen that a balance-point shall be put into place when designing a FCHEV, obtaining both favourable mass reduction and vehicle life expectancy. But overall, the results obtained from the model show vehicle mass reductions when hybridising, which increases the validity of hybridising for mass.

2.2 Class 8 HGV

Figure 8 presents the mass distributions for a heavy goods FCHEV, FCEV, or BEV under different HDs and cell operating powers. It can be seen with a 0.2 HD for MPML and NPML, hybridisation increases the power systems mass by 18% and 20%, respectively, when compared to a full BEV setup, which, if minimal system mass is the aim of hybridisation renders these solutions unfeasible. In addition to the 0.2 HD, a 3% increase in mass is also seen within the 0.4 HD when operating at NPML. Aside from the 0.2 and 0.4 HD, the trend is that higher HDs result in lower power systems mass for HGVs in a similar manner to the results seen previously.

Table 9 shows the increase or decrease of mass of the power systems of different HDs for the four scenarios explored in terms

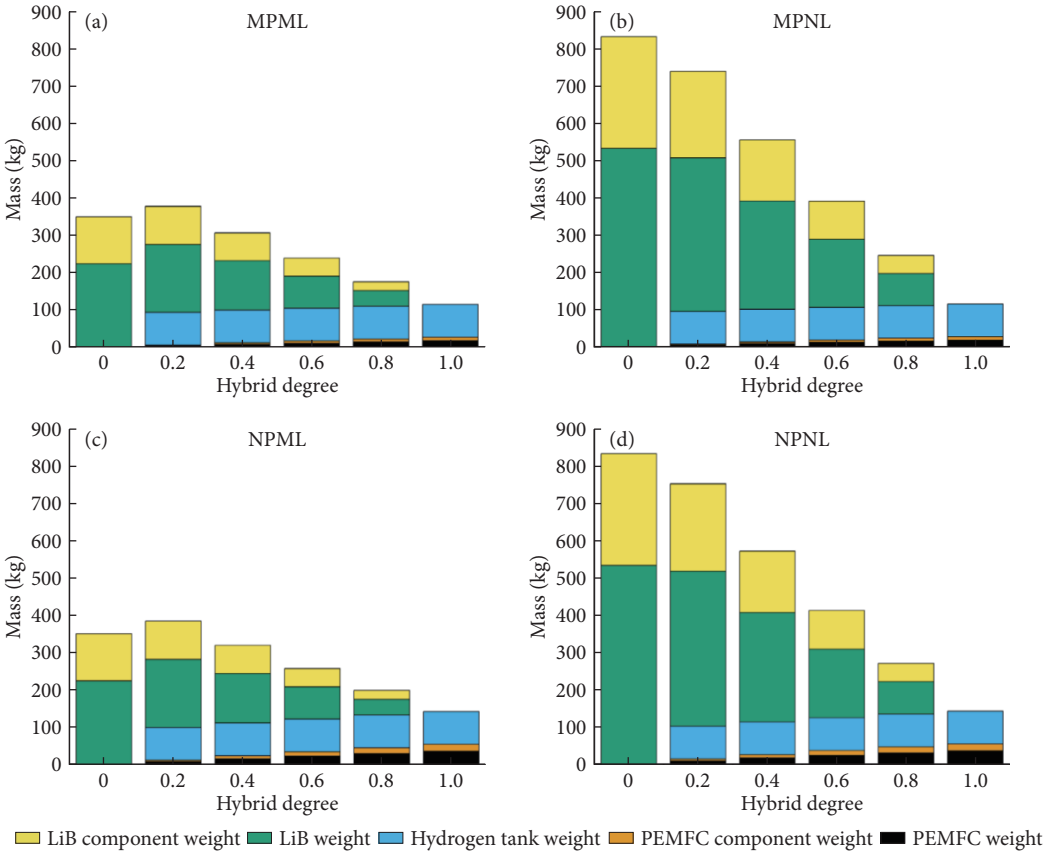

Figure 7 Power system mass distributions for a LDV FCHEV and FCEV scenario under different cell operating powers. (**a**) MPML (**b**) MPNL (**c**) NPML (**d**) NPNL.

Table 8 Percentage power systems mass increase or reduction (%) of various HDs and cell operating power when compared to a full BEV in a LDV scenario. Positive nomenclature suggests an increase in mass while negative nomenclature suggests a decrease in mass

Cell operating power	Hybridisation degree				
	0.2	0.4	0.6	0.8	1.0
MPML	8	−12	−32	−50	−67
MPNL	−11	−33	−53	−71	−86
NPML	10	−9	−27	−43	−59
NPNL	−10	−31	−51	−68	−83

of percentage when compared to a full BEV. Mass reductions range from 38% to 61% for the 0.8 HD when compared to the full BEV, illustrating the benefit of hybridising to reduce the gross vehicle mass. The mass reductions for this common HD is not as significant as compared to the LDV scenario, but is still capable of reducing the mass by more than half (61% and 58% reduction) of that of a BEV. This would require cell operating power setups of MPNL and NPNL. As highlighted previously, MPNL scenario is unlikely to be optimal to maximise the lifetime of the system and therefore would likely be assessed in the broader context of vehicle operation. However, NPNL may be a viable option if a manufacturer is looking to prolong the life of power sources for as long as possible, with some sacrifices in increased weight. The total power systems mass of a NPNL 0.8 HD setup is 1592 kg; when comparing this to a commercial heavy-goods BEV's battery pack mass of 2293 kg[36], as outlined in Table 4, the mass is still less. The heaviest possible power systems option for the 0.8 HD would still be lighter than a heavy-goods BEV's battery pack.

As for the optimal hybrid configuration of NPML, any HD over 0.6 would result in a power systems mass less than that of the full BEV counterpart and the estimated commercial LiB HGV's pack mass of 2293 kg[36].

2.3 Bus

Figure 9 presents the mass distributions for a FCHEV, FCEV, or BEV bus under different HDs and cell operating powers. Slightly different from the LDV and HGV scenarios, an increase in mass can only be seen with the NPML 0.2 HD configuration when compared to a full BEV setup; all other configurations show improvements in mass reduction as the HD increases.

Table 10 shows the increase or decrease of mass of the power systems of different HDs and cell operating power in terms of percentage when compared to a full BEV. Mass reductions range from 50% to 71% for the 0.8 HD when compared to the full BEV. The total power systems mass of a NPNL 0.8 HD setup is 583.37 kg; the mass is almost reduced by half when comparing this to a commercial ICEV bus's engine mass of 1093 kg[47], as outlined in Table 4. Even if adopting the NPNL cell operating power configuration for the 0.8 HD, the system mass would still be lighter than an ICEV bus's engine. Any HD over 0.6 would result in a power systems mass less than that of the full BEV counterpart and the estimated commercial LiB HGV's pack mass of 2293 kg[36].

3 Conclusions

This research, featuring the self-built MATLAB model HybeMass, has thoroughly examined the HD and cell operating

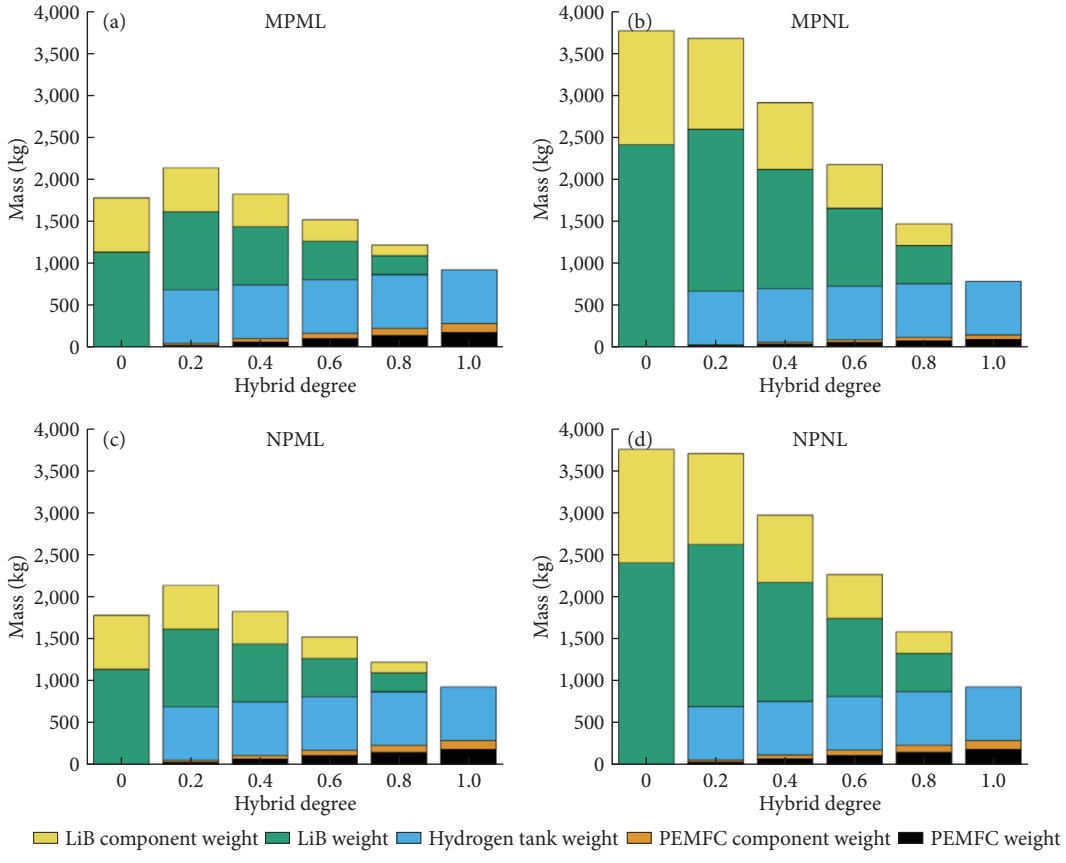

Figure 8 Power system mass distributions for a heavy-goods FCHEV and FCEV scenario under different cell operating powers. (**a**) MPML (**b**) MPNL (**c**) NPML (**d**) NPNL.

Table 9 Percentage power systems mass increase or reduction (%) of various HDs and cell operating power when compared to a full BEV in a HGV scenario. Positive nomenclature suggests an increase in mass while negative nomenclature suggests a decrease in mass

Cell operating power	Hybridisation degree				
	0.2	0.4	0.6	0.8	1.0
MPML	18	−1	−20	−38	−56
MPNL	−2	−23	−42	−61	−79
NPML	20	3	−14	−31	−48
NPNL	−1	−21	−40	−58	−75

power, establishing the necessary parameters for PEMFC and LiB cell numbers, as well as the overall power system and GVM. The implementation of a novel system mass feedback loop has enabled the automatic adjustment of the required power demand based on the changing mass of the system. This adaptive approach identifies the optimal HD, crucial for minimising vehicle mass—a pivotal design factor contributing to extended range. The evaluation extended to transient drive cycles, allowing for the estimation of power demands in diverse scenarios for LDVs, Class 8 HGVs, and buses. To ensure precision, the model accounts for parasitic component masses, auxiliary power draw, and efficiency losses in the relevant systems.

For most vehicle scenarios, a HD of 0.4 or more would result in a lesser power systems mass when compared to a full BEV. MPML cell operating power configuration would provide the lightest power systems while having the lowest durability. MPNL disregards the electrochemical benefits of PEMFCs and LiBs and is not a recommended setup; though mass reductions can still be seen with this configuration. NPML utilises the advantageous electrochemical properties of both PEMFC and LiB, and is considered a balance point for maintaining both feasible mass configuration and vehicle durability. NPNL is the 'safest' choice in terms of vehicle durability, but results in the most mass. This would be a good setup if a manufacturer's goal is to produce 'longer-lasting' vehicles. However, even with the NPNL hybridisation setup, the mass of the power systems is still less than that of a full BEV.

The HybeMass model developed here is a useful tool to enable improve the efficiency of FCHEV component sizing for automotive manufacturers and researchers. The novel system weight feedback loop eliminates the need to estimate the vehicles accurate GVM and power requirements *a priori*, instead calculating the number of PEMFC and LiB cells required alongside the total power requirements. The model has been demonstrated for different scenarios of automotive, namely LDV, HGV, and bus, across different HDs and operating powers; allowing the user to identify viable configurations depending on the vehicle design goals and purpose. Further by introducing simple modifications to the input the model can be deployed across any vehicle class and type. The model acts as a quick visualisation, elimination and calculation step prior to hardware-in-the-loop testing or bench testing of individual PEMFC or battery cells and will support wider efforts to accelerate the electrification of transport in academia and industry. For future work, a suitable ratio can be applied to adjust the hydrogen tank weight estimation between different hybrid degrees.

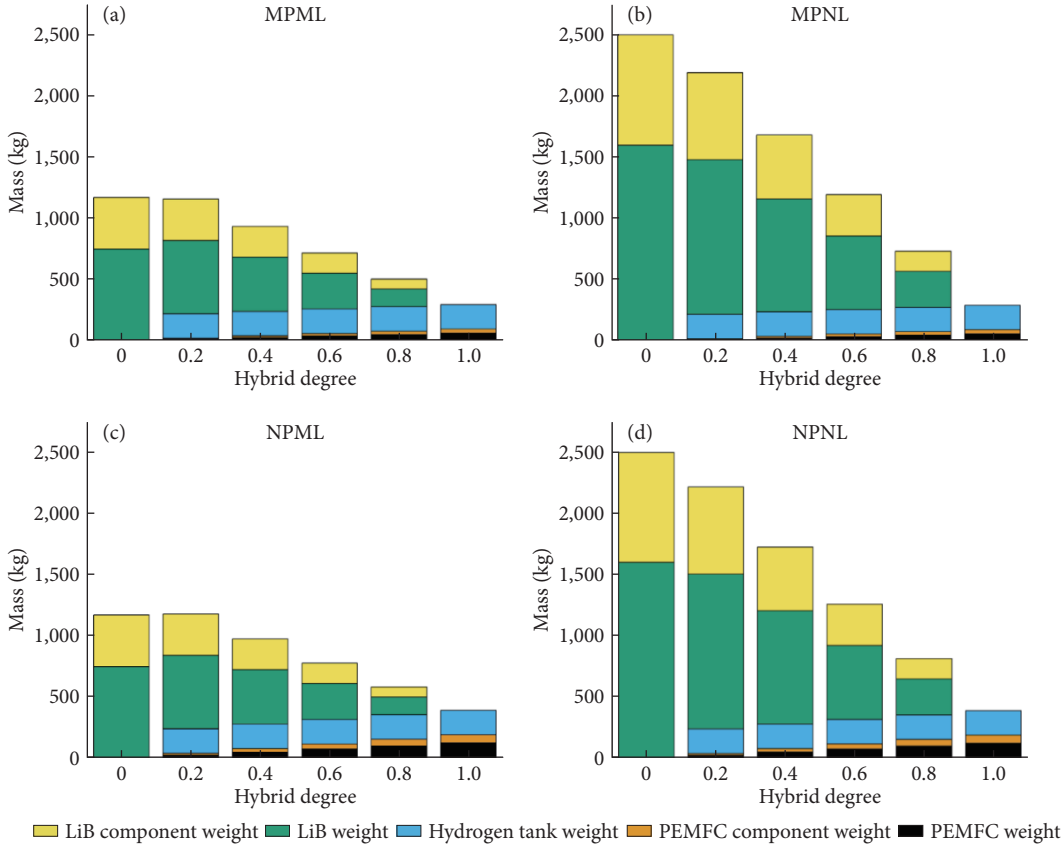

Figure 9 Power system mass distributions for a heavy-goods FCHEV and FCEV scenario under different cell operating powers. (**a**) MPML (**b**) MPNL (**c**) NPML (**d**) NPNL.

Table 10 Percentage power systems mass increase or reduction (%) of various HDs and cell operating power when compared to a full BEV in a bus scenario. Positive nomenclature suggests an increase in mass while negative nomenclature suggests a decrease in mass

Cell operating power	Hybridisation degree				
	0.2	0.4	0.6	0.8	1.0
MPML	−1	−20	−39	−57	−75
MPNL	−12	−33	−52	−71	−88
NPML	1	−21	−34	−50	−66
NPNL	−11	−31	−50	−67	−84

Article history

Received: 23 February 2024; Revised: 22 March 2024; Accepted: 27 March 2024

Additional information

Declaration of competing interest

The authors have no competing interests to declare that are relevant to the content of this article.

References

[1] Jackson, N., Morgan, R., Brett, D., Brandon, N. (2021). Fuel Cell Roadmap 2020 Narrative Report. Accessed on Nov 07 2023. Available at https://www.apcuk.co.uk/wp-content/uploads/2021/09/https___www.apcuk_.co_.uk_app_uploads_2021_02_Exec-summary-Technology-Roadmap-Fuel-Cells-final.pdf

[2] Nassif, G. G., de Almeida, S. C. A. (2020). Impact of powertrain hybridization on the performance and costs of a fuel cell electric vehicle. *International Journal of Hydrogen Energy*, 45: 21722–21737.

[3] Behera, A. (2022). Fuel cells recycling. In: Song, H., Nguyen, T. A., Yasin, G. Eds. *Nanotechnology in Fuel Cells*. Elsevier.

[4] Automotive Council UK, Advanced Propulsion Centre (2021). Electrical energy storage roadmap 2020. Narrative Report. Available at file:///C:/Users/Administrator/Downloads/https-__www.apcuk_.co_.uk_app_uploads_2021_02_Exec-summary-Technology-Roadmap-Electrical-Energy-Storage-final.pdf

[5] Gray, N., McDonagh, S., O'Shea, R., Smyth, B., Murphy, J. D. (2021). Decarbonising ships, planes and trucks: An analysis of suitable low-carbon fuels for the maritime, aviation and haulage sectors. *Advances in Applied Energy*, 1: 100008.

[6] Pollet, B. G., Staffell, I., Shang, J. L. (2012). Current status of hybrid, battery and fuel cell electric vehicles: From electrochemistry to market prospects. *Electrochimica Acta*, 84: 235–249.

[7] Yang, J. D., Millichamp, J., Suter, T., Shearing, P. R., Brett, D. J. L., Robinson, J. B. (2023). A review of drive cycles for electrochemical propulsion. *Energies*, 16: 6552.

[8] Marx, N., Hissel, D., Gustin, F., Boulon, L., Agbossou, K. (2017). On the sizing and energy management of an hybrid multistack fuel cell–Battery system for automotive applications. *International Journal of Hydrogen Energy*, 42: 1518–1526.

[9] de Almeida, S. C. A., Kruczan, R. (2021). Effects of drivetrain hybridization on fuel economy, performance and costs of a fuel cell hybrid electric vehicle. *International Journal of Hydrogen Energy*, 46: 39404–39414.

[10] Liu, B., Zhang, H., Zhu, S. (2016). An incremental V-model process

for automotive development. In: Proceedings of the 2016 23rd Asia-Pacific Software Engineering Conference (APSEC), Hamilton, New Zealand.

[11] Cai, Q., Brett, D. J. L., Browning, D., Brandon, N. P. (2010). A sizing-design methodology for hybrid fuel cell power systems and its application to an unmanned underwater vehicle. *Journal of Power Sources*, 195: 6559–6569.

[12] Zhang, Y., Zhang, C., Huang, Z., Xu, L., Liu, Z., Liu, M. (2019). Real-time energy management strategy for fuel cell range extender vehicles based on nonlinear control. *IEEE Transactions on Transportation Electrification*, 5: 1294–1305.

[13] Luca, R., Whiteley, M., Neville, T., Shearing, P. R., Brett, D. J. L. (2022). Comparative study of energy management systems for a hybrid fuel cell electric vehicle - A novel mutative fuzzy logic controller to prolong fuel cell lifetime. *International Journal of Hydrogen Energy*, 47: 24042–24058.

[14] Snoussi, J., Ben Elghali, S., Benbouzid, M., Mimouni, M. (2018). Auto-adaptive filtering-based energy management strategy for fuel cell hybrid electric vehicles. *Energies*, 11: 2118.

[15] Hwang, H. Y. (2020). Developing equivalent consumption minimization strategy for advanced hybrid system-II electric vehicles. *Energies*, 13: 2033.

[16] Garcia, P., Fernandez, L. M., Garcia, C. A., Jurado, F. (2010). Energy management system of fuel-cell-battery hybrid tramway. *IEEE Transactions on Industrial Electronics*, 57: 4013–4023.

[17] Torreglosa, J. P., Jurado, F., García, P., Fernández, L. M. (2011). Hybrid fuel cell and battery tramway control based on an equivalent consumption minimization strategy. *Control Engineering Practice*, 19: 1182–1194.

[18] Ahmadi, S., Bathaee, S. M. T., Hosseinpour, A. H. (2018). Improving fuel economy and performance of a fuel-cell hybrid electric vehicle (fuel-cell, battery, and ultra-capacitor) using optimized energy management strategy. *Energy Conversion and Management*, 160: 74–84.

[19] Yuan, X. H., Yan, G. D., Li, H. T., Liu, X., Su, C. Q., Wang, Y. P. (2022). Research on energy management strategy of fuel cell–battery –supercapacitor passenger vehicle. *Energy Reports*, 8: 1339–1349.

[20] Andreasen, S. J., Ashworth, L., Sahlin, S., Becker Jensen, H. C., Kær, S. K. (2014). Test of hybrid power system for electrical vehicles using a lithium-ion battery pack and a reformed methanol fuel cell range extender. *International Journal of Hydrogen Energy*, 39: 1856–1863.

[21] Kim, M., Sohn, Y. J., Lee, W. Y., Kim, C. S. (2008). Fuzzy control based engine sizing optimization for a fuel cell/battery hybrid minibus. *Journal of Power Sources*, 178: 706–710.

[22] Wang, Y., Moura, S. J., Advani, S. G., Prasad, A. K. (2019). Optimization of powerplant component size on board a fuel cell/battery hybrid bus for fuel economy and system durability. *International Journal of Hydrogen Energy*, 44: 18283–18292.

[23] KoteswaraRao K, V., Naga Srinivasulu, G. (2019). Modeling, downsizing, and performance comparison of a fuel cell hybrid mid-size car with FCEV for urban and hill road driving cycles. *International Journal of Green Energy*, 16: 115–124.

[24] Argonne National Laboratory (2016). Fuel cell electric truck (FCET) component sizing. Available at https://www.hydrogen.energy.gov/docs/hydrogenprogramlibraries/pdfs/review16/tv032_vijayagopal_2016_o.pdf

[25] Atwood, P., Gurski, S., Nelson, D. J., Wipke, K. B. (2001). Degree of hybridization modeling of a fuel cell hybrid electric sport utility vehicle. SAE Technical Paper 2001-01-0236.

[26] Feng, L., Chang, T. C., Guo, W., Xie, Y. C., Zheng, L. P. (2020). Optimal system parameters and hybrid ratio for fuel cell hybrid electric vehicles. *Sensors and Materials*, 32: 1593–1607.

[27] Pielecha, I. (2022). Modeling of fuel cells characteristics in relation to real driving conditions of FCHEV vehicles. Energies, 15: 6753.

[28] Partridge, J. S., Wu, W., Bucknall, R. W. G. (2020). Investigation on the impact of degree of hybridisation for a fuel cell supercapacitor hybrid bus with a fuel cell variation strategy. *Vehicles*, 2: 1–17.

[29] Bendjedia, B., Rizoug, N., Boukhnifer, M., Bouchafaa, F., Benbouzid, M. (2018). Influence of secondary source technologies and energy management strategies on energy storage system sizing for fuel cell electric vehicles. *International Journal of Hydrogen Energy*, 43: 11614–11628.

[30] Fotouhi, A., Shateri, N., Shona Laila, D., Auger, D. J. (2021). Electric vehicle energy consumption estimation for a fleet management system. *International Journal of Sustainable Transportation*, 15: 40–54.

[31] Yang, X., Liu, L. (2022). Analysis of the influence of passenger load on bus energy consumption a vehicle-engine combined model-based simulation framework. *Scientific Reports*, 12: 14535.

[32] Barelli, L., Bidini, G., Ottaviano, P. A., Pelosi, D. (2019). Vanadium redox flow batteries application to electric buses propulsion: Performance analysis of hybrid energy storage system. *Journal of Energy Storage*, 24: 100770.

[33] Cousins, K., Zhang, R. (2019). Highly porous organic polymers for hydrogen fuel storage. *Polymers*, 11: 690.

[34] Toyota UK (2023). Toyota mirai technical specifications. Accessed on Oct 11 2023. Available at https://media.toyota.co.uk/wp-content/uploads/sites/5/pdf/220203M-Mirai-Tech-Spec.pdf

[35] Lohse-Busch, H., Richards, B., Loiselle-Lapointe, A. (2018). Technology assessment of a fuel cell vehicle: 2017 Toyota mirai energy systems division. Accessed on Oct 11 2023. Available at https://publications.anl.gov/anlpubs/2018/06/144774.pdf

[36] Bethoux, O. (2020). Hydrogen fuel cell road vehicles and their infrastructure: An option towards an environmentally friendly energy transition. *Energies*, 13: 6132.

[37] Perrotta, F., Parry, T., Neves, L. C., Buckland, T., Benbow, E., Mesgarpour, M. (2019). Verification of the HDM-4 fuel consumption model using a Big data approach: A UK case study. *Transportation Research Part D: Transport and Environment*, 67: 109–118.

[38] Verbruggen, F. J. R., Hoekstra, A., Hofman, T. (2018). Evaluation of the state-of-the-art of full-electric medium and heavy-duty trucks. In: Proceedings of the 31th International Electric Vehicle Symposium & Exhibition (EVS), Kobe,Japan.

[39] Moch, J. M. (2019). Environmental implications and policy challenges for bringing long-haul electric trucks into China: The Case of the Tesla Semi. Available at www.belfercenter.org/ENRP

[40] DAF (2023). PACCAR MX-13 coach & bus engine. Available at https://www.dafcomponents.com/en/products/paccar-daf-engines/daf-mx-13-coach-and-bus-engine

[41] Electric Vehicle Database (2022). Tesla Model 3 Long Range Dual Motor. Available at https://ev-database.org/uk/car/1591/Tesla-Model-3-Long-Range-Dual-Motor

[42] Kim, Y. S., Roh, S. W. (2016). Product specification rechargeable lithium ion battery model: INR21700 M50 18.20 Wh. Accessed on Nov 10 2023. Available at https://www.dnkpower.com/wp-content/uploads/2019/02/LG-INR21700-M50-Datasheet.pdf

[43] Yang, X. G., Liu, T., Wang, C. Y. (2021). Thermally modulated lithium iron phosphate batteries for mass-market electric vehicles. *Nature Energy*, 6: 176–185.

[44] Blagojević, I., Mitić, S. (2018). Hydrogen as a vehicle fuel. *Mobility and Vehicle Mechanics*, 44: 37–49.

[45] Purnima, P., Jayanti, S. (2020). Optimal sizing of a fuel processor for auxiliary power applications of a fuel cell-powered passenger car. *International Journal of Hydrogen Energy*, 45: 26005–26019.

[46] Lawrence, C. P., ElShatshat, R., Salama, M. M. A., Fraser, R. A. (2016). An efficient auxiliary system controller for fuel cell electric vehicle (FCEV). *Energy*, 116: 417–428.

[47] Meng, K., Zhou, H., Chen, B., Tu, Z. (2021). Dynamic current cycles effect on the degradation characteristic of a H_2/O_2 proton exchange membrane fuel cell. *Energy*, 224: 120168.